FED-Vol. 229, Laser Anemometry
ASME 1995

LASER DOPPLER VELOCIMETRY FLOW MEASUREMENTS IN THE ROTATING FRAME INSIDE THE PASSAGE OF A LOW SPECIFIC SPEED MODEL CENTRIFUGAL PUMP IMPELLER

F.C. Visser and J.B. Jonker
Faculty of Mechanical Engineering
University of Twente
P.O. Box 217, 7500 AE ENSCHEDE
The Netherlands

ABSTRACT

This paper describes two-component laser doppler velocimetry flow measurements of the relative velocity field inside the passage of a low specific speed model centrifugal pump impeller. The velocity components were measured in the rotating frame, in radial and circumferential direction, by means of a co-rotating Helium-Neon forward-scatter reference-beam laser doppler velocimeter. The experiments were performed on a nine-bladed shrouded perspex test impeller of simple two-dimensional design, fitted out with sixty-degree backward-leaning logarithmic spiral blades. Velocities were obtained at two passage cross-sections, and at several midheight radial and circular cross-passage trajectories. The measurement results distinctly confirmed the potential flow character of the bulk of the passage flow. In particular, the presence of the relative eddy was corroborated.

NOMENCLATURE

b = impeller passage breadth
d_p = diameter of tracer particles
$F(-)$ = hypergeometric function
h = axial depth of impeller
n = number of blades
Q_v = volume flow rate
R = dimensionless radius
r = radius
r_1 = inner blade radius
r_2 = outer blade radius
$\tilde{r}$ = blade fitted dimensionless radius
s = blade-fitted curvilinear coordinate
$\tilde{s}$ = dimensionless curvilinear coordinate
TI = turbulence intensity
$u, \dot{u}$ = velocity and acceleration of particles
$u_\perp$ = doppler velocity
Δu = slip velocity of seed particles
w_r = radial velocity component
w_t = streamwise velocity component
w_ϕ = circumferential velocity component
z = axial coordinate
β = blade angle
$\tilde{\phi}$ = blade fitted dimensionless polar coordinate
μ = equivalent space-chord ratio
ν = kinematic viscosity of working fluid
ρ = density of working fluid
ρ_p = density of tracer particles
τ_0, τ_β = prerotation factor
Φ = volume flow rate coefficient
Φ_s = volume flow rate at shockless entry
Ω = angular speed of impeller

Subscripts

ps = pressure side
ss = suction side

INTRODUCTION

Detailed knowledge of flow patterns occurring in impeller passages is of cardinal importance in the design of centrifugal pumps and for the prediction of their hydraulic behaviour. To that end numerous theoretical

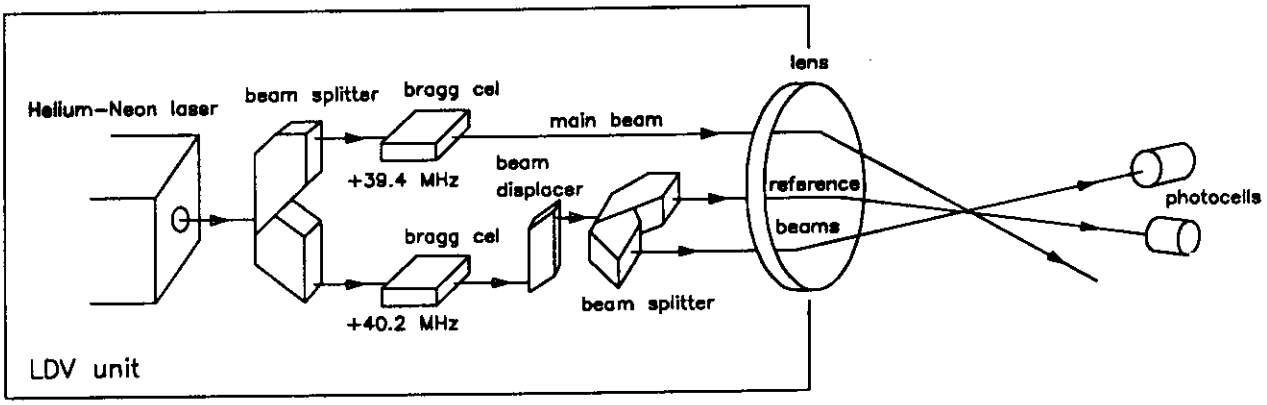

Fig. 1 Arrangement of the LDV unit and photocells (Delft Hydraulics Laboratory - The Netherlands)

and experimental studies have been conducted in the past. The theoretical investigations in this field mainly involved analytical studies and numerical computations on individual components and simplified configurations (see for instance Visser et al. 1994 and Badie et al. 1994), whereas experimental work concerned for most cases the study of hydraulic behaviour and performance of complete machines. Experiments on the individual components, like the impeller, have thus far been limited to a few studies only (see also Abramian & Howard 1994*a,b*). Consequently, proper data for verification of theoretically computed impeller passage flow fields is scarcely available.

Because of this lack of data for verification, an experiment was set up to measure the velocity field in the passages of a low-specific speed (model) centrifugal pump impeller using laser doppler velocimetry. This measurement technique was utilised in such a way that passage velocities could be measured directly, that is without the employment of an image-derotator device (unlike e.g. Fagan and Selbach 1986, and Abramian and Howard 1994*a,b*). To that end the laser doppler velocimeter co-rotated with the impeller. Furthermore, the laser doppler velocimeter measured simultaneously the radial and circumferential component of the (relative) velocity. Other experimenters in this field utilised one-component laser doppler velocimetry and, hence, had to conduct separate sessions in order to get two-component velocity information.

Due to the fact that derotator optics could be omitted, the laser doppler velocimeter employed offered information of the passage flows better than the systems reported to date; e.g. the one of Abramian & Howard (1994*a,b*). The measurements obtained readily provided distinct information of the flow patterns with respect to the rotating frame of reference, which enabled

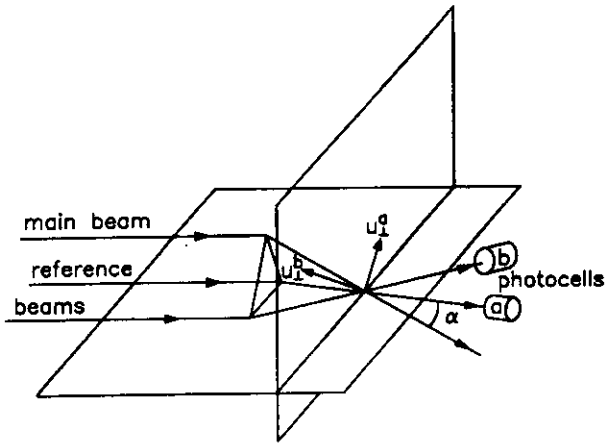

Fig. 2 Principle of the two-dimensional reference-beam forward-scatter LDV system

immediate identification of flow phenomena like the relative eddy.

EXPERIMENTAL TECHNIQUE

Seeding

Since laser doppler velocimetry (LDV) is based on measuring the motion of (seed) particles it is important that these particles follow the fluid without significant slip. This implies that the particles should be (preferably) neutrally buoyant and as small as possible.

For the present work we utilised natural seeding, while demineralised tap water was the working fluid. According to Adrian (1991) the slip of the particles can be estimated by

$$|\Delta u| = \frac{\rho_p}{\rho} \frac{d_p^2}{36\nu} |\dot{u}| \qquad (1)$$

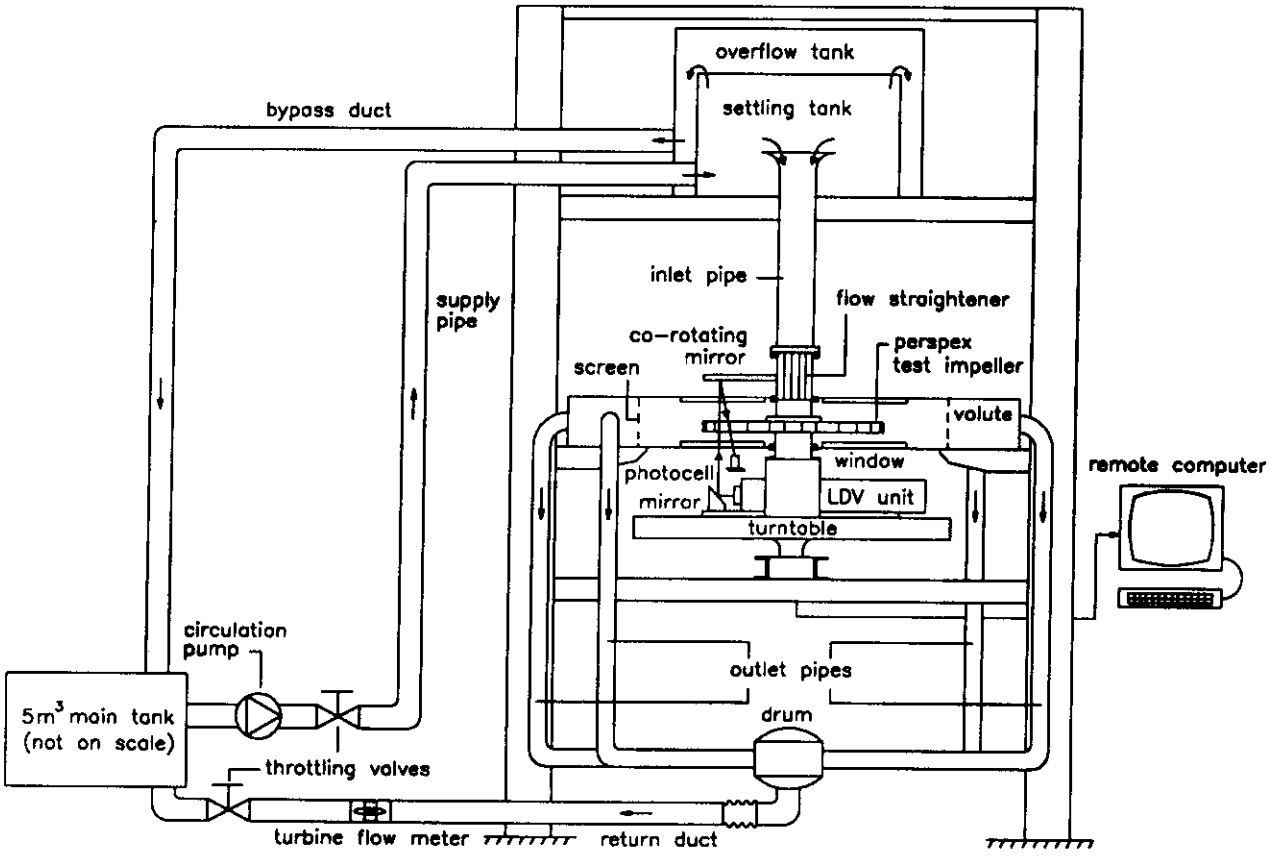

Fig. 3 Diagram of the test rig

in which - with subscript "p" denoting particle properties - ρ is density and ν is kinematic viscosity of the working fluid, d is diameter and Δu and $\dot{u}$ are slip velocity and acceleration. Evaluating (1), taking $d_p \approx 1\ \mu$m and $\rho_p \approx \rho$, we find a negligible slip ($\Delta u < 10^{-3}$ mm/s, based on $|\dot{u}| \approx u^2/r$ and taking into account that u and r are of the order 1 m/s and 0.1 m).

LDV Equipment

The LDV system used in the experimental facility was a two-component forward-scatter reference-beam arrangement (Figs. 1 and 2) with combined counter-tracker signal processor which was developed by the Delft Hydraulics Laboratory - The Netherlands. Strong points of the arrangement are 1) high data density at good signal-to-noise ratio, 2) low laser power, and 3) simple realisation of two-dimensional system. A minor imperfection is that for the reference beam arrangement the intensity fluctuations of the laser beam must be very small, since these fluctuations are also in the reference beam which is always shining on the detector. So, if these fluctuations are not outside the doppler frequency band or very small, they can be misinterpreted as doppler signals and cause false velocity information.

The set-up employed could measure velocity components between -1.43 m/s and +1.43 m/s. In the LDV unit (see Fig. 1), a 6 mW Helium-Neon laser provided a laser beam which was bisected by a beam splitter into a (80 %) high-intensity main beam and a (20 %) low-intensity secondary beam. Two bragg cells arranged for a frequency shift of 39.4 MHz to the main beam and 40.2 MHz to the secondary beam, establishing an actual frequency shift of 0.8 MHz. This pre-shift eliminated directional ambiguity, so that not only the absolute value but also the direction of the velocity components could be measured. A beam displacer corrected the alignment of the secondary beam after the bragg cell, and a second beam splitter divided the beam in two identical reference beams. The two reference beams and the main beam were focussed with a 400 mm focal-depth lens, so that they intersected in one point, yielding two measurement volumes with a length of 6.5 mm each. Two photocells detected the scatter of the particles moving through the measurement volumes (Fig. 2), which sig-

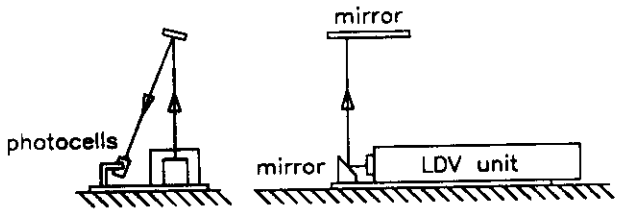

Fig. 4 Arrangement of the LDV system

nals were sent to a signal processing unit.

The processing unit contained two frequency trackers, each of them controlled by a counter. The counters provided the capture range of the trackers and the matching of the signal frequency. This way the small capture range of the frequency trackers was overcome, while the high response rate could still be benefited. The output signal of each tracker was a (DC) voltage level between -10 V and +10 V, which was stored digitally and processed on a remote computer.

With the LDV arrangement two velocity components could be obtained simultaneously. In each measurement volume the velocity component $u_\perp$ perpendicular to the bisector of the main beam and the respective reference beam was measured. At each measurement location the (two) signals representing the instantaneous velocity components were each sampled two thousand times, at a 30 Hz sample frequency. From these samples the ensemble averaged mean and variance were computed.

EXPERIMENTAL FACILITY

Test Rig

The experiments were performed in the test rig illustrated schematically in Fig. 3. This open-loop test facility was specifically designed, so that throughput and impeller speed could be set independently, enabling a wide range of operating points.

The horizontally mounted impeller was fixed rigidly on the turntable, which had a 0-100 rpm angular speed range. The volume flow rate through the impeller was controlled by means of a throttling valve in the return duct and could be set from 0 to 20 l/s.

The impeller discharged in an oversized volute, which was equipped with special hardened glass windows and four outlets. Downstream disturbances were stemmed by a cylindrical screen placed around the impeller. A flow straightener was installed in the impeller inlet pipe.

The frequency-controlled circulation pump fed the settling tank, such that the test rig operated under overflow conditions; that is, the settling tank was flooded and a small flux of water was bypassed to the main

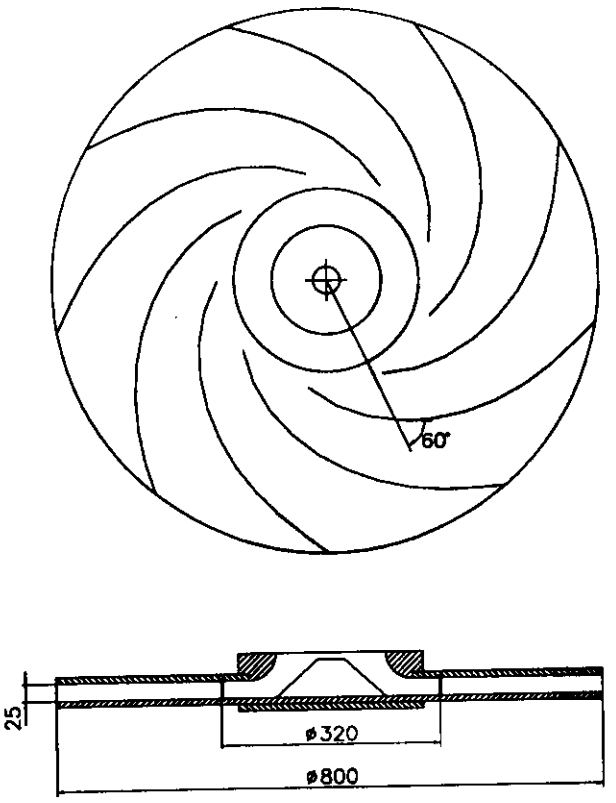

Fig. 5 Nine-bladed test impeller with sixty-degree logarithmic spiral blades (dimensions in mm)

tank. The settling tank was open to atmosphere.

The LDV unit was stationed on the turntable, and co-rotated with the impeller (see also Fig. 4). A mirror placed in front of the LDV unit deflected the three laser beams, so that the measurement volumes were positioned in the impeller passage. A second mirror, attached to the inlet-shroud-configuration and thus co-rotating with the impeller, reflected the reference beams onto the photocells on the turntable. The photocells sent their signals to the processing unit, also mounted on the turntable. The output signal of the processing unit was transmitted over a slip-ring arrangement to a remote computer, where it was subsequently stored and processed.

Test Impeller

The LDV experiments were conducted while having installed a nine-bladed, shrouded, model impeller of simple two-dimensional design. This model was equipped with sixty-degree backward-leaning logarithmic spiral blades with 0.4 inlet-to-outlet radius ratio, and had 25 mm constant axial depth (see also Fig. 5).

The impeller was made entirely of perspex to meet

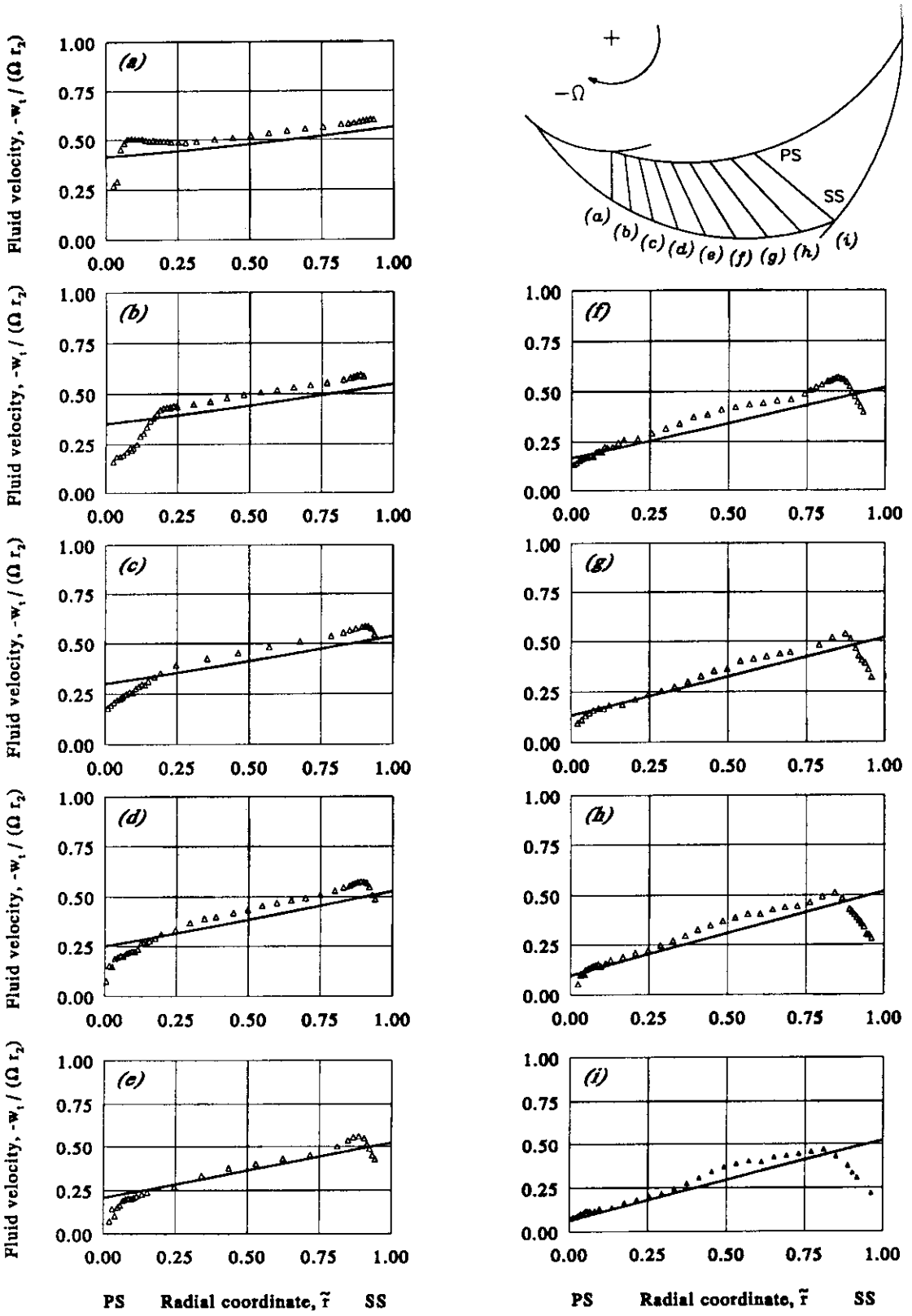

Fig. 6 Measured and computed mid-height passage velocities at nine equidistantly distributed pressure-to-suction side radial trajectories ($\Phi = -0.117$); (a) $R_{ps} = 0.4$, (b) $R_{ps} = 0.434$, (c) $R_{ps} = 0.467$, (d) $R_{ps} = 0.501$, (e) $R_{ps} = 0.534$, (f) $R_{ps} = 0.568$, (g) $R_{ps} = 0.601$, (h) $R_{ps} = 0.635$, (i) $R_{ps} = 0.668$

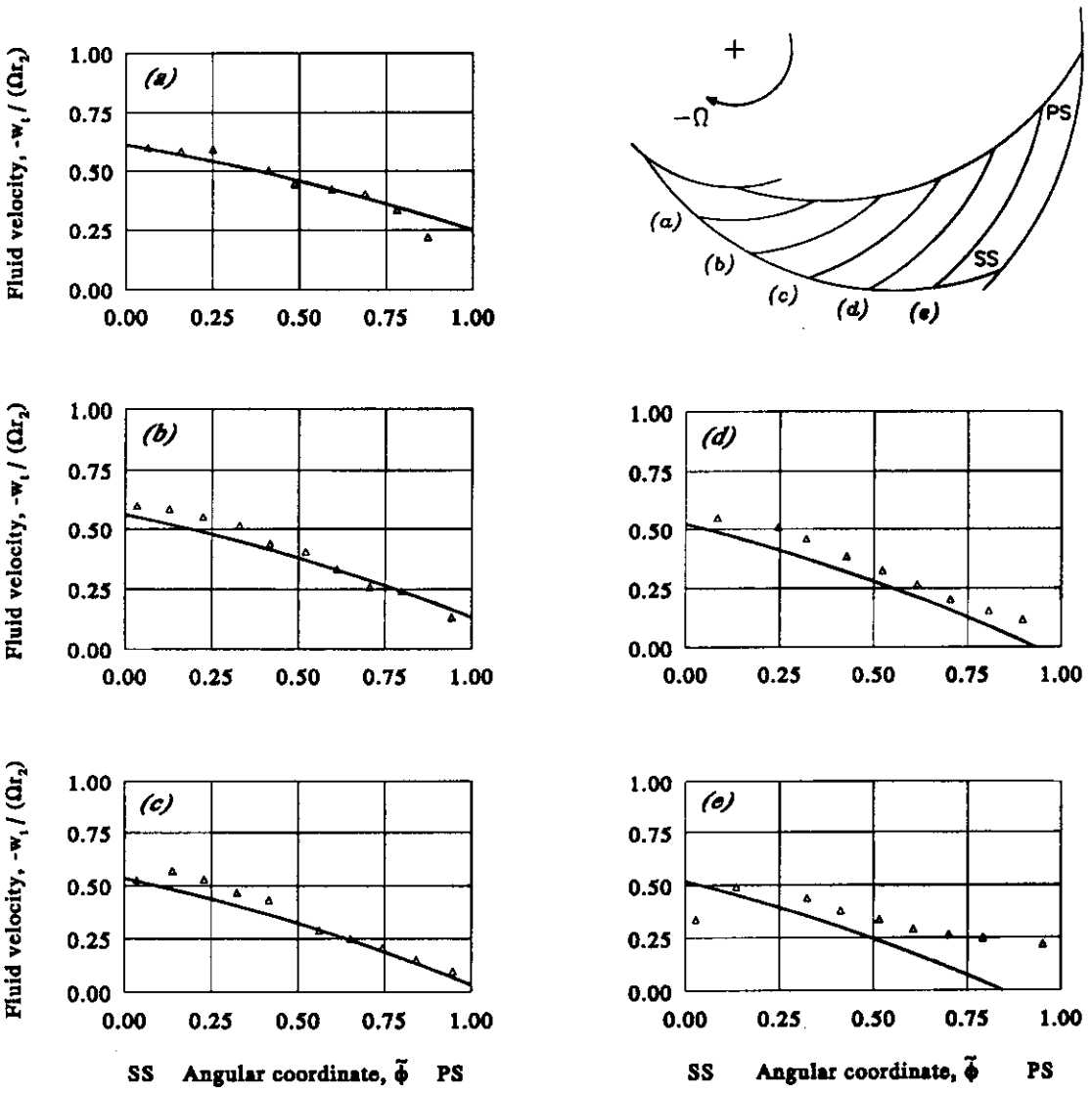

Fig. 7 Measured and computed mid-height suction-to-pressure side passage velocities at (a) 0.5 r_2, (b) 0.6 r_2, (c) 0.7 r_2, (d) 0.8 r_2, and (e) 0.9 r_2 radial distance ($\Phi = -0.117$)

the demand of optical accessibility. The blades were cut from 2 mm sheet and were recessed in slots milled in hub and shroud. The hub and shroud were made of 10 mm sheet, and the inlet eye was machined out of 40 mm sheet. The resulting impeller assembly was joined together with acrylate glue.

The impeller had a design flow rate coefficient $\Phi = -0.117$, where

$$\Phi = \frac{Q_v}{2\pi\Omega r_2^2 h} \tag{2}$$

in which Q_v is volume flow rate, r_2 is outer blade radius, Ω is angular speed, and h is axial depth of the impeller. It should be recognised that the direction of revolution of the impeller can be either clockwise (i.e. $\Omega < 0$) or counterclockwise (i.e. $\Omega > 0$), representing backward or forward curvature respectively. A positive throughput combined with backward leaning blades therefore gives $\Phi < 0$, strange as it may seem. This convention has been adopted from Visser et al. (1994).

The design point was computed on the basis of two-dimensional potential flow analysis, such that the relative flow would run smoothly on the leading edge with no velocity discontinuities. This point of operation, commonly termed (condition of) shockless entry, will be designated by Φ_s. The value of this shockless-entry volume flow rate coefficient depends solely on the dimensions and blade shape of the impeller (assuming a two-dimensional logarithmic spiral design).

In line with the results of Visser et al. (1994), and making the assumption that there is no prewhirl, we used

$$\Phi_s = -\tau_\beta \left(\frac{r_1}{r_2}\right)^2 cotan(\beta) \tag{3}$$

in which we estimated

$$\tau_\beta = 1 + (\tau_0 - 1)cos(\beta) \tag{4}$$

where

$$\tau_0 = \left(\frac{2}{1+\mu^{\frac{1}{2}}}\right)^{4/n} F\left(\frac{2}{n}, \frac{2}{n}; 1; \left(\frac{1-\mu^{\frac{1}{2}}}{1+\mu^{\frac{1}{2}}}\right)^2\right) \tag{5}$$

with $F(-) = {}_2F_1(-)$ is (Gauss) hypergeometric function, n is number of blades, β is blade angle, and $\mu = (r_1/r_2)^n$ is equivalent space-chord ratio. For $n = 9$, $\beta = \pi/3$ and an inner-to-outer blade radius ratio $r_1/r_2 = 0.4$ we obtain $\Phi_s = -0.117$. This value of Φ_s meets the demand of $-\Phi \geq -\Phi_m$ where Φ_m is the flow rate coefficient minimally required to avoid reverse flow in the impeller passages. For nine sixty-degree backward-leaning logarithmic spiral blades we have that $\Phi_m \sim -0.105$ as $\mu \to 0$; see Visser et al. (1994).

Lastly, we note that the impeller was designed to run at 32 rpm. At this angular speed, the Reynolds number based on the impeller outlet diameter and tip speed equals 10^6.

RESULTS

Mid-Height Passage Flow

Figs. 6 and 7 show the streamwise velocity component w_t measured at mid-height along radial and circular cross-passage trajectories. This velocity component has been obtained form the measurement results, employing

$$w_t = w_r cos(\beta) + w_\phi sin(\beta) \tag{6}$$

where w_r and w_ϕ are the measurement results in radial and circumferential direction respectively. The plots are presented in dimensionless form, for which we have made use of blade-fitted coordinates $(\tilde{r}, \tilde{\phi})$ defined by

$$\tilde{r} = \frac{r - r_{ps}}{r_{ss} - r_{ps}} \tag{7}$$

$$\tilde{\phi} = \frac{\phi - \phi_{ss}}{\phi_{ps} - \phi_{ss}} \tag{8}$$

where the respective subscripts denote suction side (ss) and pressure side (ps); see also Fig. 8.

Besides the measurement result, the plots also show theoretical values, which are computed from an asymptotic expansion that is founded on the assumption of incompressible potential flow. This expansion reads (Visser et al., 1994)

$$\frac{w_t}{\Omega r_2} \sim \frac{R}{sin(\beta)} \left(\frac{sinh(t)}{t} e^{t(2\tilde{\phi}-1)} - 1\right) + \frac{\Phi}{Rcos(\beta)} \tag{9}$$

as $\mu \to 0$, in which $R = r/r_2$ and $t = \pi sin(2\beta)/n$. Relation (9) readily yields the values along circular cross-passage trajectories. Values along radial cross-passage trajectories are computed from (9) by using the relationship

$$\tilde{\phi} = 1 - \frac{ntan(\beta)}{2\pi} ln\,(R/R_{ps}) \tag{10}$$

describing radial cross-passage trajectories in blade-fitted coordinates.

The plots (Figs. 6 and 7) display good agreement between measured and computed values. The potential flow character of the impeller passage flow is distinctly present. In particular, the presence of the relative eddy is confirmed by higher values of the streamwise velocity on the suction side of the blades and near stagnation flow close to the pressure side of the blades. Prior study

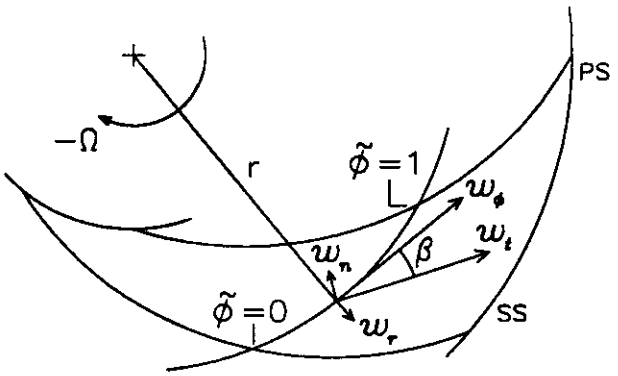

Fig. 8 Passage velocities

(Visser & Jonker, 1995) of the impeller passage flow, using particle image velocimetry, sustains these findings.

Near the blade surfaces we notice a departure from the potential flow character due to the effect of viscosity. Especially, near the blade suction side, and, in particular, close to the trailing edge, we experience a thick non-separated boundary layer.

To illustrate this effect of viscosity we have computed a boundary layer thickness (δ_{ss}), representing the arc length at which $\partial w_t/\partial r = 0$, based on the data plotted in Fig. 6. The result of this exercise is shown in dimensionless form in Fig. 9, for which we have employed a blade-fitted curvilinear coordinate ($\tilde{s}$) defined by

$$\tilde{s} = \frac{s cos(\beta)}{r_2 - r_1} \qquad (11)$$

where s is the distance travelled along a blade from the leading edge forth. Furthermore, δ_{ss} is plotted in respect of the impeller passage breadth $b = 2\pi r/n$. Also note that in the special case of logarithmic spiral blades $s = (r - r_1)/cos(\beta)$, and, hence, $\tilde{s} = (r - r_1)/(r_2 - r_1)$.

The computed values of δ_{ss} strongly suggest a logarithmic boundary layer development. Employing the method of least-squares, we find

$$ln\left(\frac{\delta_{ss}}{b}\right) = -3.5 + 2.25\,\tilde{s} \qquad (12)$$

which relation has been plotted also in Fig. 9.

Lastly, completing the discussion of the subject, it is emphasized that despite the adverse pressure gradient we do not experience boundary layer separation. Moreover, we observe a diminishing boundary layer thickness along the blade pressure side.

Cross-Sectional Impeller Passage Flow

Fig. 10 gives an overview of the cross-sectional passage velocity measured at $R = 0.5$ and $R = 0.7$. Figs. 11

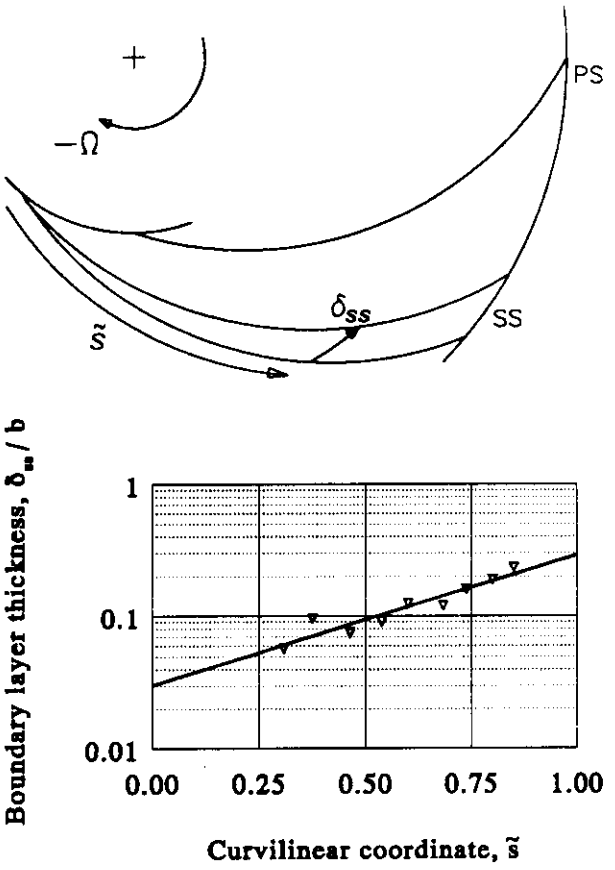

Fig. 9 Boundary layer development along the blade suction side ($\Phi = -0.117$)

and 12 show the respective hub-to-shroud measurement results, and the theoretical values according to (9). Again we notice proper agreement between measurement results and (two-dimensional) potential flow values. Moreover, it is seen that the passage flow displays a two-dimensional behaviour.

Additionally, it is noted that the measurements across the impeller passage height did not reveal secondary cross flows, despite the low passage aspect ratio of the test impeller. Roth & Johnston (1976) - inspired by the results of Moore (1973) - specifically mentioned that they used a *high* aspect ratio. Present measurement results indicate that this seems to be rather redundant.

Turbulence Intensity

Turbulence is customarily understood to mean the random motion of a fluid, and is normally contrasted with the steady flow. In order to quantify this perception it is common practice to relate the specific kinetic

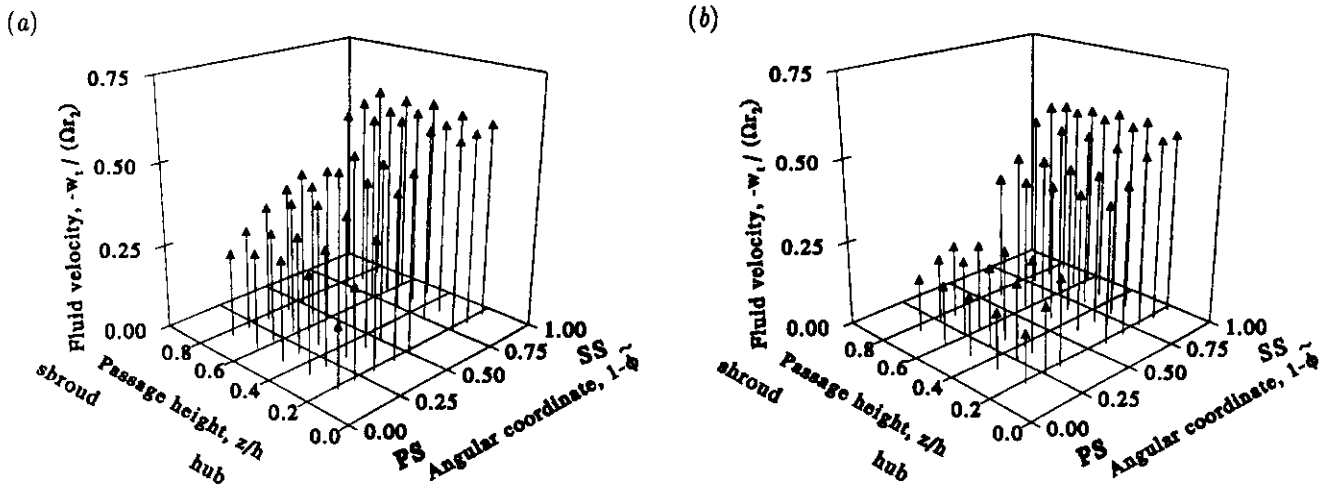

Fig. 10 Passage velocities measured at (a) 0.5 r_2, and (b) 0.7 r_2 radial distance ($\Phi = -0.117$)

energy (k) of the turbulent fluctuations to the mean velocity ($\bar{v}$). This way we get the turbulence intensity

$$TI = k/(\bar{v})^2 \tag{13}$$

Obedient to this definition we have computed a turbulence intensity, based on the ensemble averaged mean and the RMS value of the velocity fluctuations, according to

$$TI = \frac{1}{2}\frac{(w_r')^2 + (w_\phi')^2}{(\bar{w}_r)^2 + (\bar{w}_\phi)^2} \tag{14}$$

in which the prime denotes the RMS value of the velocity fluctuations, and the overbar denotes the averaged mean. Abramian & Howard (1994b) and Flack et al. (1992) employed a similar definition, except for the fact that they took the square root of the right-hand side of (14).

The results computed by (14) are plotted in Fig. 13. The plots display a decline of the turbulence intensity from pressure side to suction side, until the (suction side) boundary layer is entered. This behaviour was also reported by Abramian & Howard (1994b). Inside the boundary layer the turbulence intensity is seen to intensify rapidly. It should, however, be recognised that this behaviour is largely due to the fact that locally (mean) fluid velocities become quite small. Likewise, the turbulence intensity is strongly influenced by the fact that the pressure side (mean) fluid velocity lies considerably below the suction side value. Hence, one should be extremely cautious when drawing conclusions from the behaviour of the turbulence intensity.

CONCLUDING REMARKS

A co-rotating laser doppler velocimetry flow measurement system has been used to study the flow in the passages of a low specific speed model centrifugal pump impeller of simple two-dimensional design. The measurement results have been compared with theoretical two-dimensional potential-flow-based values, which showed that the impeller passage flow is well-described by two-dimensional potential flow theory. In particular, the presence of the relative eddy, which is responsible for the slip effect in centrifugal impellers, has been confirmed by higher values of the passage velocity at the blade suction side and near stagnation flow velocity at the blade pressure side. Furthermore, in line with classical flow theory, a departure from potential flow values was experienced near the blades surfaces.

The results presented shed light on the real-fluid character of - low specific speed - impeller passage flows, and may serve to improve practical design of centrifugal pumps. Application of the findings to complete machines is justified, since at the design point and somewhat on either side of it the influence of the impeller housing is not marked. Only at flow rates much lower and particularly much higher than the design point significant deviations from free-impeller performance will emerge.

ACKNOWLEDGEMENTS

The authors gratefully acknowledge the support by SHELL The Netherlands.

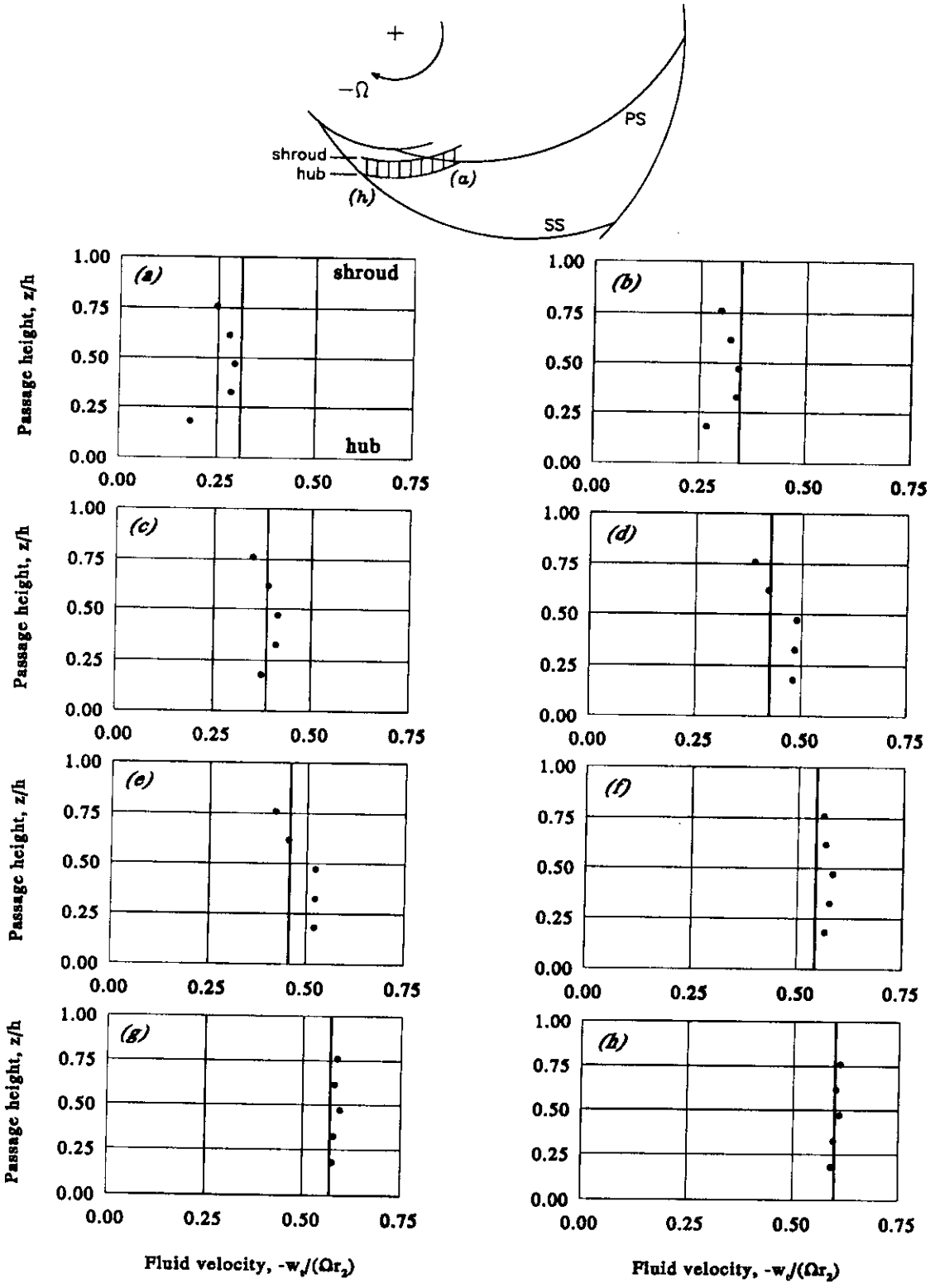

Fig. 11 Measured and computed hub-to-shroud passage velocities at 0.5 r_2 radial distance ($\Phi = -0.117$); (*a*) $\tilde{\phi} = 0.87$, (*b*) $\tilde{\phi} = 0.79$, (*c*) $\tilde{\phi} = 0.69$, (*d*) $\tilde{\phi} = 0.59$, (*e*) $\tilde{\phi} = 0.51$, (*f*) $\tilde{\phi} = 0.25$, (*g*) $\tilde{\phi} = 0.16$, (*h*) $\tilde{\phi} = 0.06$

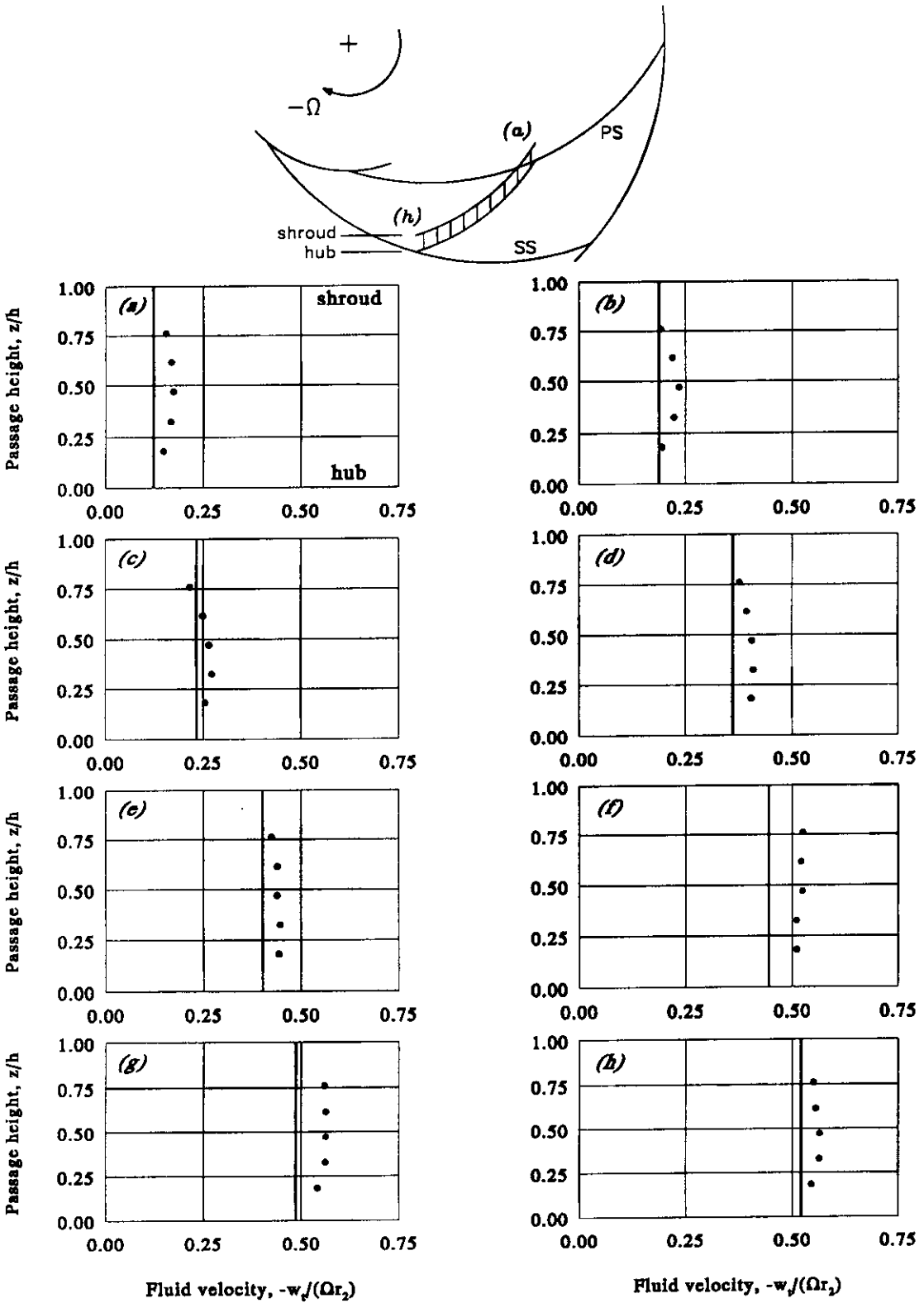

Fig. 12 Measured and computed hub-to-shroud passage velocities at 0.7 r_2 radial distance ($\Phi = -0.117$): (*a*) $\tilde{\phi} = 0.86$, (*b*) $\tilde{\phi} = 0.75$, (*c*) $\tilde{\phi} = 0.67$, (*d*) $\tilde{\phi} = 0.42$, (*e*) $\tilde{\phi} = 0.33$, (*f*) $\tilde{\phi} = 0.23$, (*g*) $\tilde{\phi} = 0.13$, (*h*) $\tilde{\phi} = 0.03$

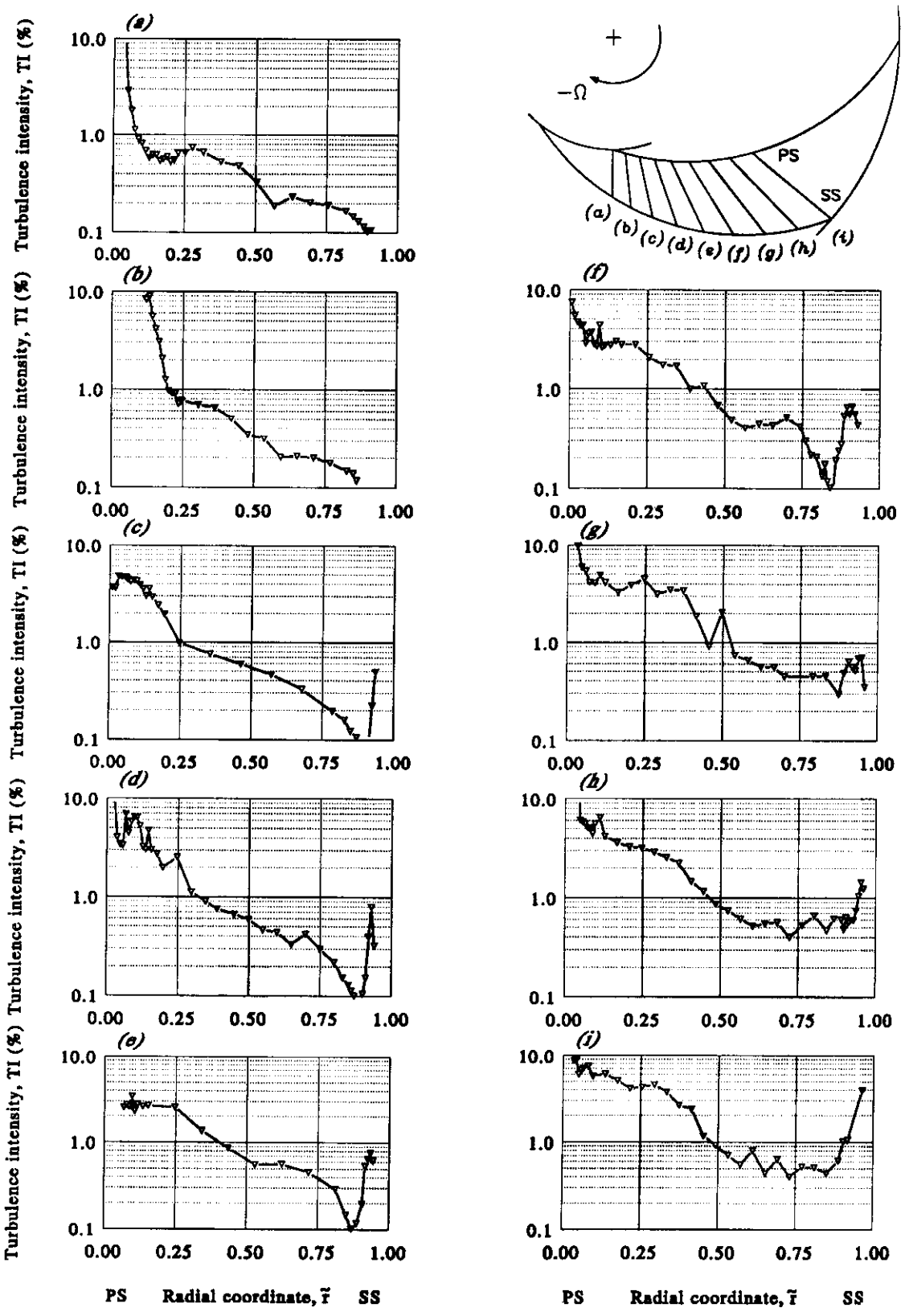

Fig. 13 Turbulence intensities, according to (14), at nine equidistantly distributed mid-height pressure-to-suction side radial trajectories ($\Phi = -0.117$); (a) $R_{ps} = 0.4$, (b) $R_{ps} = 0.434$, (c) $R_{ps} = 0.467$, (d) $R_{ps} = 0.501$, (e) $R_{ps} = 0.534$, (f) $R_{ps} = 0.568$, (g) $R_{ps} = 0.601$, (h) $R_{ps} = 0.635$, (i) $R_{ps} = 0.668$

REFERENCES

ABRAMIAN, M. & HOWARD, J.H.G. 1994*a* A rotating laser-doppler anemometry system for unsteady relative flow measurements in model centrifugal impellers. *J. Turbomachinery* **116**, 260-268.

ABRAMIAN, M. & HOWARD, J.H.G. 1994*b* Experimental investigation of the steady and unsteady relative flow in a model centrifugal impeller passage. *J. Turbomachinery* **116**, 269-279.

ADRIAN, R.J. 1991 Particle-imaging techniques for experimental fluid mechanics. *Annu. Rev. Fluid Mech.* **23**, 261-304.

BADIE, R., JONKER, J.B. & VAN DEN BRAEMBUSSCHE, R.A. 1994 Finite element calculations and experimental verifications of the unsteady potential flow in a centrifugal volute pump. *Int. J. Num. Meth. Fluids.* **19**, 1083-1102.

FAGAN, W. & SELBACH, H. 1986 Laser 2 focus flow measurements in the absolute and rotating frame inside the blade row of an axial flow fan. *Proceedings of the third international symposium on applications of laser anemometry to fluid mechanics, July 7-9, Lisbon, Portugal.*

FLACK, R.D., MINER, S.M. & BEAUDOIN, R.J. 1992 Turbulence measurements in a centrifugal pump with a synchronously orbiting impeller. *J. Turbomachinery* **114**, 350-359.

MOORE, J. 1973 A wake and eddy in a rotating, radial-flow passage. Part 1: experimental results. *J. Engng Power* **95**, 205-212.

ROTHE, P.H. & JOHNSTON, J.P. 1976 Effects of system rotation on the performance of two-dimensional diffusers. *J. Fluids Engng* **98**, 422-430.

VISSER, F.C., BROUWERS, J.J.H. & BADIE, R. 1994 Theoretical analysis of inertially irrotational and solenoidal flow in two-dimensional radial-flow pump and turbine impellers with equiangular blades. *J. Fluid Mech.* **269**, 107-141.

VISSER, F.C. & JONKER, J.B. 1995 Investigation of the relative flow in low specific speed model centrifugal pump impellers using sweep-beam particle image velocimetry. *Proceedings of the seventh international symposium on flow visualization, September 11-14, Seattle, Washington, USA.*